ACS APPLIED MATERIALS & INTERFACES

Research Article

www.acsami.org

Superior Hybrid Cathode Material Containing Lithium-Excess Layered Material and Graphene for Lithium-Ion Batteries

Ke-Cheng Jiang,[†] Xing-Long Wu,[†] Ya-Xia Yin,[†] Jong-Sook Lee,[‡] Jaekook Kim,[‡] and Yu-Guo Guo*[,†,‡]

[†]Key Laboratory of Molecular Nanostructure and Nanotechnology, and Beijing National Laboratory for Molecular Sciences (BNLMS), Institute of Chemistry, Chinese Academy of Sciences (CAS), Beijing, 100190, P. R. China

[‡]School of Materials Science and Engineering, Chonnam National University (WCU), Gwangju 500-757, Republic of Korea

Supporting Information

ABSTRACT: Graphene-wrapped lithium-excess layered hybrid materials ($Li_2MnO_3{\cdot}LiMO_2$, M = Mn, Ni, Co, hereafter abbreviated as LMNCO) have been synthesized and investigated as cathode materials for lithium-ion batteries. Cyclic voltammetry measurement shows a significant reduction of the reaction overpotential in benefit of the graphene conducting framework. The electrochemical impedance spectroscopy results reveal that the graphene can greatly reduce the cell resistance, especially the charge transfer resistance. Our investigation demonstrates that the graphene conducting framework can efficiently alleviate the polarization of pristine LMNCO material leading to an outstanding enhancement in cell performance and cycling stability. The superior electrochemical properties support the fine hybrid structure design by enwrapping active materials in graphene nanosheets for high-capacity and high-rate cathode materials.

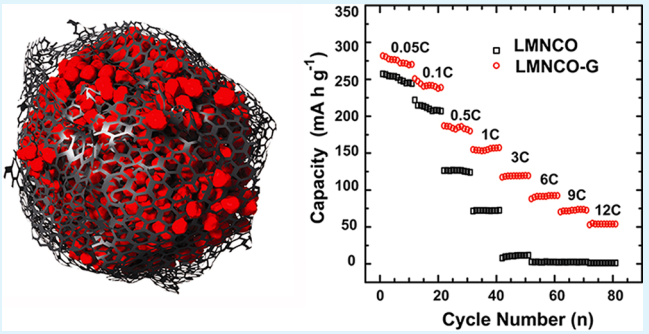

KEYWORDS: *lithium-ion batteries, hybrid materials, cathode, lithium-excess layered materials, graphene*

1. INTRODUCTION

Because of global warming and the exhaustion of fossil fuels, considerable attention has been paid to lithium-ion batteries (LIBs) targeted at their potential applications in electric vehicles (EVs) and hybrid electric vehicles (HEVs). However, the energy densities of current LIBs are much lower than that of the fuel engine as revealed by the limited drive range of current EVs. For traditional carbon-anode-based LIBs, one of the well-recognized factors to decide their energy densities are the specific capacity of the cathode material selected. Recently, lithium-excess layered materials of $Li_2MnO_3{\cdot}LiMO_2$ (M = Mn, Ni, Co, hereafter abbreviated as LMNCO) have attracted increasing interest[1−3] because of their high specific capacities up to 250 mA h g^{-1}. Compared to the widely used cathode materials such as $LiCoO_2$ (140 mA h g^{-1}),[4−6] LMNCO is also known to have the advantages including low cost and low safety risk. However, the poor rate capabilities and bad cyclability have restricted their further commercialization. The cycling performance of LMNCO is mainly limited by the side reactions on its surface such as electrolyte decomposition and transition metal dissolution. A widely used strategy to improve its cycling stability is to reduce the direct contact between active LMNCO particles and the electrolyte by coating the particles with either metal oxides or fluorides.[7−11] However, most of these surface modification materials are electronically insulated, thus leading to an increased electronic resistance on the surface, and finally resulting in a poor high-rate capability. Therefore, constructing a hybrid structure with the help of electronically conductive networks, such as carbon nanotubes,[12] carbon nanofibers,[13,14] and porous carbons,[15] becomes an promising route to improve both the cycling stability and the high-rate capability. According to the electrode kinetics: $k = k_0 \exp[\beta nF\Delta\varphi/RT]$, where k is the reaction rate constant, k_0 is the standard rate constant, β is the barrier symmetry factor, n is the number of electrons involved in the electrode reaction, F is the Faraday constant, $\Delta\varphi$ is the overpotential, R is the universal gas constant, and T is the absolute temperature. The decrease of overpotential $\Delta\varphi$ can slow down the corresponding side reaction. Considering that the electrode overpotential mainly originates from the electrochemical and concentration polarizations, it is reasonable that the improvement of the electrode conductivities as well as the decrease of the polarization will be helpful to depress the side reactions. Consequently an enhanced cycling performance can be expected. In addition, increasing the electronic conductivity can also benefit Li transportation during the fast charge−discharge processes. Therefore enwrapping cathode materials into a conductive network becomes a favorable choice to achieve better high-rate capability. Recently, graphene and its composites have been intensively investigated due to their extraordinary electrical behavior, stable chemical property, and high specific surface area.[16−20] Their excellent performances in LIBs have been observed.[21−26] It is suggested that graphene can

Received: July 2, 2012
Accepted: August 29, 2012
Published: August 29, 2012

be a promising electron-conducting component for constructing hybrid cathode materials of LMNCO.

2. EXPERIMENTAL SECTION

The Li-excess layered material of $Li(Li_{0.2}Mn_{0.54}Ni_{0.13}Co_{0.13})O_2$ (LMNCO) was synthesized by a sol−gel method using citric acid as the chelating agent. Stoichiometric amounts of lithium acetate, manganese acetate, nickel acetate and cobalt acetate were chosen as the starting materials to prepare the precursor. All salts were dissolved in distilled water and added dropwisely into citric acid solution under continuous stirring. After the dissolution of all salts, the temperature of solution was raised to 80 °C and a continuous stirring was applied until a clear viscous gel was formed. The gel was dried in an oven at 100 °C to obtain the precursor powder. After heated at 450 °C in air for 5 h, the powder was ground, pelletized, and then calcined at 900 °C for 12 h in air.

To get well dispersed graphene sheets, natural graphite was oxidized using a modified Hummers method,[23] followed by a reduction in H_2/Ar stream at 700 °C for 2 h. The as-obtained graphene sheets with 7−10 layers are in the size of 4−6 μm as confirmed by HRTEM and TEM images (see the Supporting Information, Figures S1 and S2).

For preparation of the graphene-wrapped Li-$(Li_{0.2}Mn_{0.54}Ni_{0.13}Co_{0.13})O_2$ composite, 50 mg of graphene was dispersed in 25 mL ethanol and ultrasonicated for 2 h, then 950 mg LMNCO powder was added to the suspension and magnetically stirred at 50 °C for 4 h. The as-obtained mixture was dried overnight at 90 °C. The mass percentage of graphene in the final hybrid material is 4.9 wt % as measured by TGA (see the Supporting Information, Figure S3).

X-ray diffraction (XRD) measurements of the LMNCO powder were performed using a Philips PW3710 with filtered Cu Kα radiation (Rigaku D/max-2500). Raman measurements were carried out using a DXR Raman Microscope (Thermao Fisher Scientific Inc.) with a laser wavelength of 514.5 nm. SEM (JEOL 6701F, operating at 10 kV) and TEM (JEOL 4000EX, operating at 400 kV) were used to investigate the morphology and size of the LMNCO powder and the LMNCO-G composite.

Electrochemical measurements were performed using Swagelok-type cells assembled in an argon-filled glovebox. A mixture of active material, carbon black (CB), and poly(vinyl difluoride) (PVDF) at a weight ratio of 80: 10: 10 was pasted on an Al foil to prepare the working electrodes. The loading mass of active materials is about 10 mg cm^{-2}. The specific capacity of the hybrid is calculated based on the mass of LMNCO. Pure lithium foil was used as a counter electrode. A glass fiber (GF/D) from Whatman was used as the separator. The electrolyte consisted of a solution of 1 M $LiPF_6$ in ethylenecarbonate (EC)/dimethylcarbonate (DMC)/diethylcarbonate (DEC) (1: 1: 1 in wt%) obtained from Tianjing Jinniu Power Sources Material Co. Ltd. Galvanostatic cycling of the assembled cells was carried out using an Arbin BT2000 system between the voltage limits of 2.0−4.7 V (vs Li^+/Li). Cyclic voltammetry (CV) and electrochemical impedance spectroscopy (EIS) measurements were carried out on an Autolab PG302N at room temperature.

3. RESULTS AND DISCUSSION

Figure 1a shows the XRD patterns of the as-prepared $Li(Li_{0.2}Mn_{0.54}Ni_{0.13}Co_{0.13})O_2$ and graphene-wrapped Li-$(Li_{0.2}Mn_{0.54}Ni_{0.13}Co_{0.13})O_2$ composite (LMNCO-G). The pattern is indexed in characteristic of the O3 layered structure with weak superstructure reflections observed around 20−25°, corresponding to the Li^+ cation ordering in the transition metal layer.[27] All the reflections are from the layered oxide without any peaks for graphene due to its nanoscale size and low content. The Raman spectra of both LMNCO and LMNCO-G show peaks at 424, 477, and 590 cm^{-1} (Figure 1b). The peaks at 477 and 590 cm^{-1} are attributed to the E_g and A_{1g} vibrations of Raman-active LMNCO with the $R3\bar{m}$ symmetry, respectively. The 424 cm^{-1} peak is known to be the fingerprint vibration of the Li_2MnO_3 superlattice.[28] For LMNCO-G, intense vibrations observed at 1341 and 1586 cm^{-1} are due to the D and G bands of graphene, respectively. The result confirms the existence of graphene in the composite.

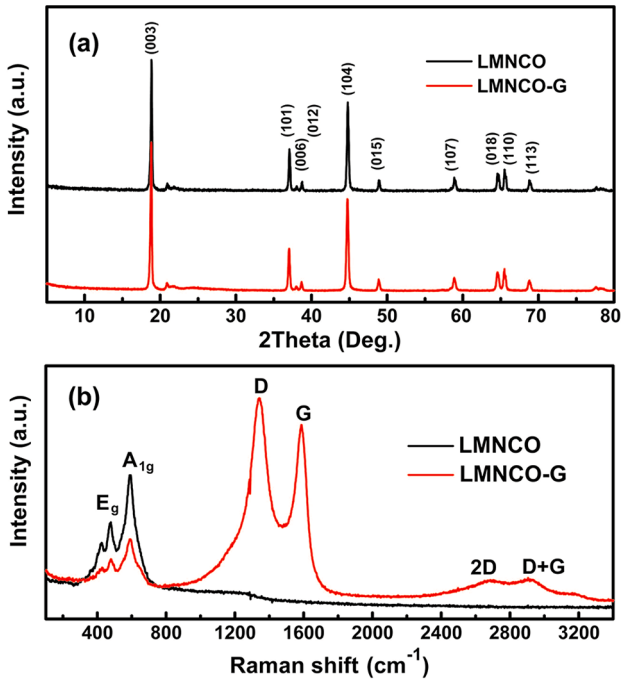

Figure 1. (a) XRD patterns and (b) Raman spectra of LMNCO and LMNCO-G.

The SEM image of the LMNCO powder reveals that the nanoparticles are in the shapes of regular polyhedrons (Figure 2a). The smooth planes on their surface indicate that these particles are highly crystalline. The SEM and TEM images of the LMNCO-G composite show that LMNCO nanoparticles with the diameters around 200−300 nm have been enwrapped

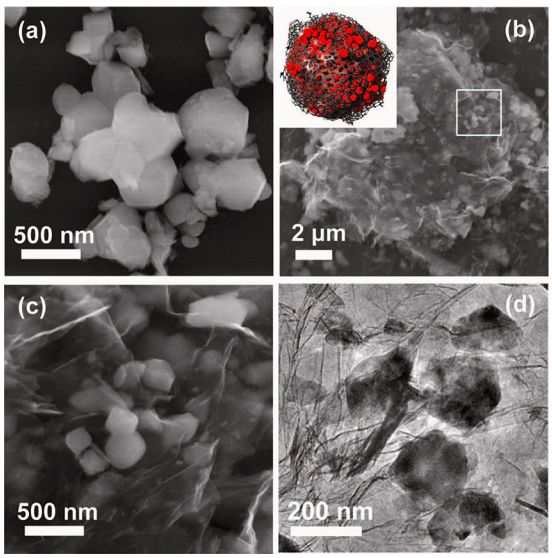

Figure 2. (a) SEM image of LMNCO and (b) SEM image of LMNCO-G. The inset shows the schematic illustration of the hybrid structure. (c) High-magnification SEM image of the selected area in panel b. (d) TEM image of LMNCO-G.

dx.doi.org/10.1021/am301202a | ACS Appl. Mater. Interfaces 2012, 4, 4858−4863

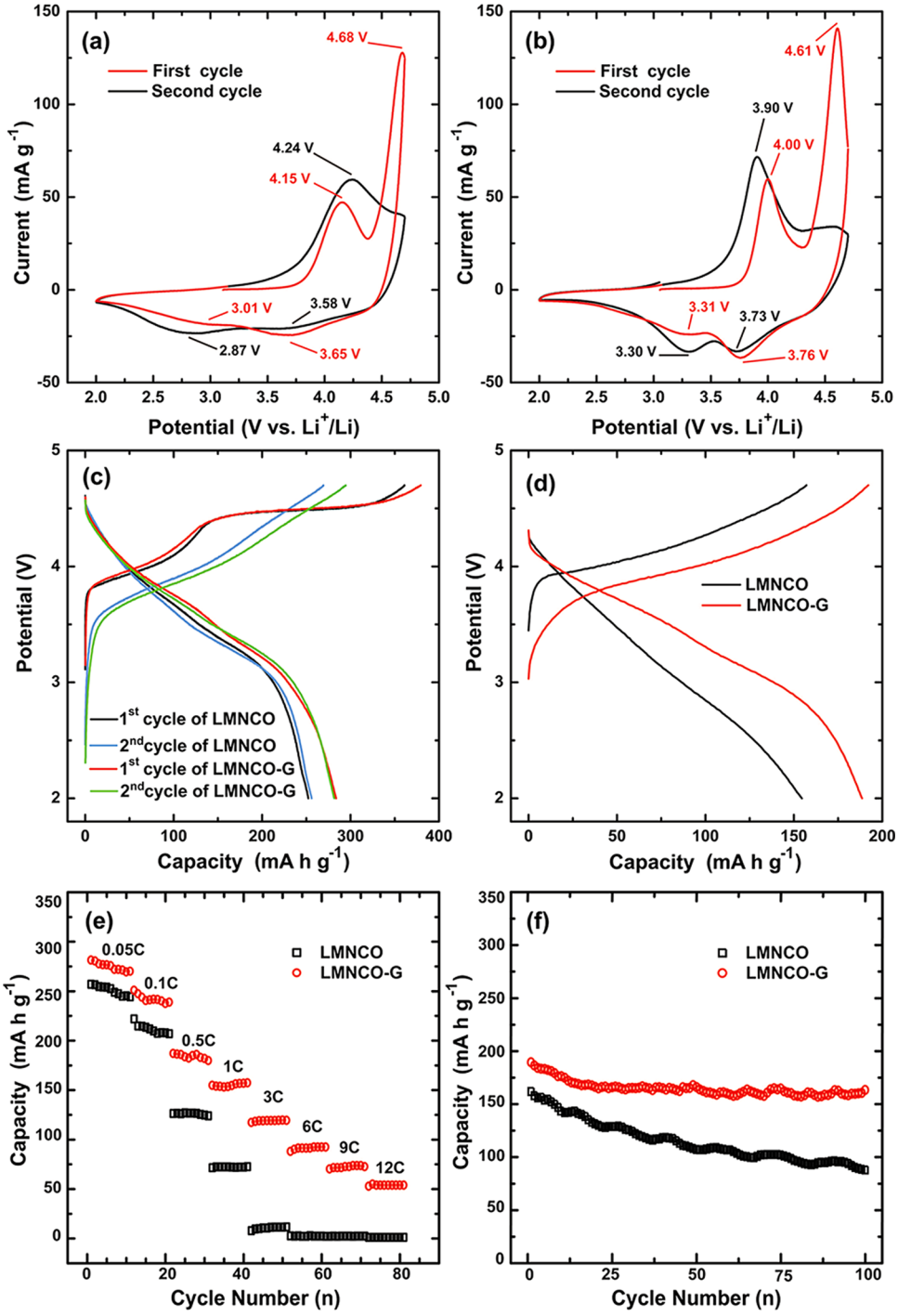

Figure 3. CV curves of (a) LMNCO and (b) LMNCO-G at a scan rate of 0.05 mV s^{-1}. (c) The first and the second charge−discharge voltage profiles of LMNCO and LMNCO-G at 0.05C. (d) The third charge−discharge voltage profiles of LMNCO and LMNCO-G at 0.5C after one initial cycle at 0.05C. (e) Rate performance of LMNCO and LMNCO-G. (f) Cycling performance (reversible discharge capacity) of LMNCO and LMNCO-G at 0.5C between the voltage limits of 2.0−4.7 V.

by flexible graphene sheets (Figure 2b−d). The LMNCO-G composite with such a hybrid structure is in the size of tens of micrometers (Figure 2b). For such hybrid nano/micro-structure, the conductive contact between the nanosized LMNCO particles and the current collector can be remarkably improved by the microscopic graphene network due to its excellent electronic conductivity, which endows the LMNCO-G composite with superior electrochemical properties.

Figure 3a and b shows the initial two cyclic voltammetry (CV) curves of the LMNCO and the LMNCO-G electrodes in the potential range of 2.0−4.7 V at a scan rate of 0.05 mV s^{-1}. In comparison with the pristine LMNCO material, the current intensities of oxidation and reduction peaks of LMNCO-G are obviously increased. The potential difference between these two peaks is smaller for the LMNCO-G electrode, indicating that the polarization of the electrode has been significantly reduced with the aid of graphene. Figure 3c shows the initial

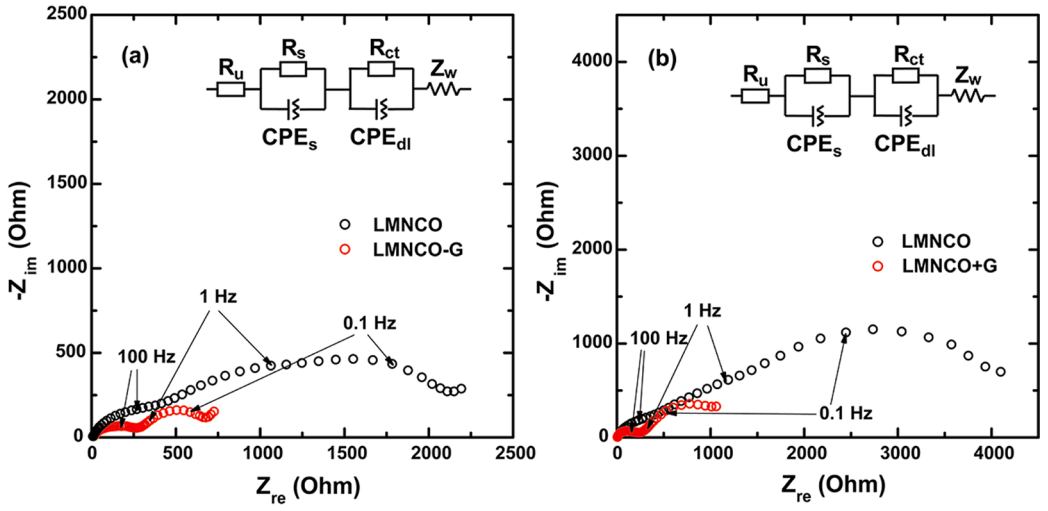

Figure 4. EIS of LMNCO and LMNCO-G recorded after the 10th cycle (a) and the 100th cycle (b) over the frequency range from 0.01 Hz to 100 kHz. In the equivalent circuit, R_u is the uncompensated ohmic resistance, representing the ohmic polarization. The resistor R_s and constant phase element CPE_s at high frequency correspond to the lithium-ion transfer through the surface layer. The R_{ct} at lower frequency correspond to the charge transfer reaction, and the CPE_{dl} can be attributed to the nonideal double layer capacitance. The Z_w represents the Warburg impedance describing the lithium ion diffusion in the bulk material.

two charge−discharge voltage profiles of LMNCO and LMNCO-G at a low rate of 0.05C (1C = 250 mA g^{-1}). A slope region of the first charging curve is observed for both electrodes, which is attributed to the extraction of Li^+ from the lithium layer. The LMNCO-G composite delivers a higher discharge capacity (~290 mA h g^{-1}) than that (~256 mA h g^{-1}) of the pristine LMNCO cathode. The initial Coulombic efficiency of the LMNCO-G (~74%) is also higher than that (~69%) of the LMNCO. It is known that the theoretical capacity of the LMNCO can be calculated as 250 mA h g^{-1} when assuming all Mn^{4+} are reduced to Mn^{3+} at first charging process and one electron reduction based on the transition metals (i.e., Co^{3+}/Co^{4+}, Ni^{3+}/Ni^{4+}, and Mn^{3+}/Mn^{4+}). In other words, 0.8 mol Li is assumed for the $Li_{1.2}Co_{0.13}Ni_{0.13}Mn_{0.54}O_2$ material which is widely used in literature.[7,8] It is found that the specific discharge capacity of the LMNCO material can exceed 250 mA h g^{-1} at 0.05C, which might be attributed to the factors that oxygen works as a reversible redox species on the electrode surface without the release of oxygen gas besides the transition metal redox reactions.[2] It has been found that the phase transformation in the two-phase region of the layered $LiNi_{1/3}Mn_{1/3}Co_{1/3}O_2$ cathode material could be greatly promoted by the sufficient electron supply provided by the graphene sheets.[29] Similarly, in the present work, the graphene sheets are expected to promote the transformation reactions at the ~4.5 V plateau during the first charging process of LMNCO, in which oxygen atoms are removed from the crystal lattice and Mn^{4+} ions are reduced to Mn^{3+} simultaneously.[2] In addition, irreversible side reactions for the LMNCO-G cathode might be depressed in the initial charging process due to the significantly reduced polarization by adding graphene sheets to LMNCO, as shown in the CV curves (see Figure 3a, b). Since Mn^{3+} ions are reversible in the following Li insertion/extraction process, the more Mn^{4+}/Mn^{3+} transformation and the less irreversible side reaction could attribute to the increased discharge capacity and Coulombic efficiency of the LMNCO-G.

Figure 3d shows the typical charge−discharge voltage profiles of LMNCO and LMNCO-G at 0.5C after one initial cycle at 0.05C. Compared with the high charge voltage plateau of about 4.20 V for the pristine LMNCO, the LMNCO-G composite exhibits a low charge voltage plateau of 3.95 V, indicating a much lowered overpotential. The lowered overpotential is in good agreement with the above CV tests. The LMNC-G cathode is expected to hold an improved high-rate capability and cycle stability as the side reactions might be depressed with the significantly reduced overpotential of $\Delta\varphi$.

To evaluate the rate performances of the pristine LMNCO material and the LMNCO-G composite, both of them were cycled from 0.05C to 12C (i.e., 12.5 mA g^{-1} to 3000 mA g^{-1}) between the voltage limits of 2.0 − 4.7 V vs Li^+/Li (Figure 3e). While the LMNCO electrode exhibits nearly no discharge capacity at 3C (completing the discharge process in 20 min), the LMNCO-G composite can still deliver a discharge capacity of about 120 mA h g^{-1}. Furthermore, the LMNCO-G composite has a discharge capacity as high as 50 mA h g^{-1} even at a very high rate of 12C. Figure 3f shows the cycling behaviors of the LMNCO and the LMNCO-G electrodes cycled at 0.5C. The corresponding Coulombic efficiency profiles are shown in Figure S4 in the Supporting Information. The efficiencies of both electrodes maintain around 100% in all cycles except for the first one, indicating their good cycling behaviors. The capacity retention is above 90% after 100 cycles for the LMNCO-G composite, which is much higher than that of 54% for the pristine LMNCO. Such a good cycling performance is not noticed in the literature. The superior high-rate capability and long-term cyclability of LMNCO-G composite demonstrate that the designed graphene-wrapped hybrid structure is effective to improve the electrochemical properties of LMNCO. To clarify the recover capabilities of the cathode materials after cycling at high rates, both the LMNCO and LMNCO-G cathodes were successively cycled at 0.05C, 0.1C, 0.5C, 1C, 3C, and 6C, and finally cycled at 0.1C (see the Supporting Information, Figure S5). The result shows that the recovery rates of LMNCO and LMNCO-G are 99% and 95%, respectively, which indicates an enhanced recover capability and stability after introducing the graphene sheets to LMNCO.

To further understand the effects of graphene in the hybrid structure on the electrochemical properties of LMNCO,

electrochemical impedance spectroscopy (EIS) spectra were measured for both the LMNCO and the LMNCO-G electrodes after the 10th and the 100th cycles (Figure 4a, b). Prior to the EIS measurements, the samples were charged to 50% state of charge (SOC) to reach an identical status. All the EIS spectra show two semicircles, which can be fit by using the equivalent circuits as shown in the insets in Figure 4a,b. The first semicircle at high frequency corresponds to the lithium-ion transfer through the surface layer, while the second semicircle at lower frequency can be attributed to the charge transfer reaction.[30] The values of parameters R_s and R_{ct} calculated by the nonlinear least-squares fitting are summarized in Table 1. It

Table 1. Resistance Values Obtained from Equivalent Circuit Fitting of Experimental Data for the LMNCO and LMNCO-G Electrodes

		R_s (Ω)	R_{ct} (Ω)
LMNCO	after the 10th cycle	271	1964
	after the 100th cycle	349	4319
LMNCO-G	after the 10th cycle	258	406
	after the 100th cycle	210	1535

can be seen that the introduction of graphene into LMNCO can decrease the values of both R_s and R_{ct}. Especially, the R_{ct} is remarkably reduced because of the improved electronic conductivity, indicating an enhancement in the kinetics and the consequent improvement in high-rate capabilities. After long time cycling, the increased resistance value of LMNCO-G composite is much less than that of pristine LMNCO, which is in consistent with the superior stability as demonstrated by the cycling tests.

4. CONCLUSIONS

In summary, we have designed and synthesized a graphene-wrapped LMNCO cathode material with superior electrochemical properties. In the hybrid cathode material, the graphene sheets serve as efficient electronically conductive frameworks benefitting from their 2D structure and outstanding electronic conductivity. The polarization of pristine LMNCO can be effectively alleviated with the help of graphene, leading to much improved high-rate capability and cyclability (capacity retention above 90% after 100 cycles) in the LMNCO-G hybrid material. The results here give clear evidence of the power of graphene to improve the cycle performance of the high-capacity lithium-excess layered cathode materials via promoted charge transfer reaction and lowered charge polarization. The hybrid structure with active cathode nanoparticles enwrapped in graphene nanosheets could also be extended to other high-energy cathode materials with either high potential or high capacity.

■ ASSOCIATED CONTENT

Supporting Information

HRTEM and TEM images of graphene sheets, TGA profile of LMNCO-G, Coulombic efficiency profiles of LMNCO and LMNCO-G cycled at 0.5C, and rate behaviors of LMNCO and LMNCO-G. This material is available free of charge via the Internet at http://pubs.acs.org.

■ AUTHOR INFORMATION

Corresponding Author

*E-mail: ygguo@iccas.ac.cn. Tel./Fax: +86-10-62557908.

Notes

The authors declare no competing financial interest.

■ ACKNOWLEDGMENTS

This work was supported by the National Basic Research Program of China (Grants 2012CB932900 and 2011CB935700), the National Natural Science Foundation of China (Grants 91127044 and 21121063), the WCU program through NRF funded by MEST (*R*32-2009-000-20074-0), and the Chinese Academy of Sciences. The authors thank Prof. A. M. Cao for helpful discussions.

■ REFERENCES

(1) Johnson, C. S.; Kim, J. S.; Lefief, C.; Li, N.; Vaughey, J. T.; Thackeray, M. M. *Electrochem. Commun.* **2004**, *6*, 1085−1091.
(2) Yabuuchi, N.; Yoshii, K.; Myung, S.-T.; Nakai, I.; Komaba, S. *J. Am. Chem. Soc.* **2011**, *133*, 4404−4419.
(3) Armstrong, A. R.; Holzapfel, M.; Novák, P.; Johnson, C. S.; Kang, S. H.; Thackeray, M. M.; Bruce, P. G. *J. Am. Chem. Soc.* **2006**, *128*, 8694−8698.
(4) Ellis, B. L.; Lee, K. T.; Nazar, L. F. *Chem. Mater.* **2010**, *22*, 691−714.
(5) Okubo, M.; Hosono, E.; Kim, J.; Enomoto, M.; Kojima, N.; Kudo, T.; Zhou, H.; Honma, I. *J. Am. Chem. Soc.* **2007**, *129*, 7444−7452.
(6) Mizushima, K.; Jones, P.; Wiseman, P.; Goodenough, J. *Mater. Res. Bull.* **1980**, *15*, 783−789.
(7) Wu, Y.; Manthiram, A. *Electrochem. Solid-State Lett.* **2006**, *9*, A221−A224.
(8) Gao, J.; Kim, J.; Manthiram, A. *Electrochem. Commun.* **2009**, *11*, 84−86.
(9) Zheng, J.; Li, J.; Zhang, Z.; Guo, X.; Yang, Y. *Solid State Ionics* **2008**, *179*, 1794−1799.
(10) Wu, Y.; Vadivel Murugan, A.; Manthiram, A. *J. Electrochem. Soc.* **2008**, *155*, A635−A641.
(11) Kim, G. Y. *J. Appl. Electrochem.* **2008**, *38*, 1477−1481.
(12) Cao, F. F.; Guo, Y. G.; Zheng, S. F.; Wu, X. L.; Jiang, L. Y.; Bi, R. R.; Wan, L. J.; Maier, J. *Chem. Mater.* **2010**, *22*, 1908−1914.
(13) Bonino, C. A.; Ji, L.; Lin, Z.; Toprakci, O.; Zhang, X.; Khan, S. A. *ACS Appl. Mater. Interfaces* **2011**, *3*, 2534−2542.
(14) Yu, Y.; Gu, L.; Wang, C.; Dhanabalan, A.; van Aken, P. A.; Maier, J. *Angew. Chem., Int. Ed.* **2009**, *48*, 6485−6489.
(15) Wu, X. L.; Jiang, L. Y.; Cao, F. F.; Guo, Y. G.; Wan, L. J. *Adv. Mater.* **2009**, *21*, 2710−2714.
(16) Ji, H.; Hao, Y.; Ren, Y.; Charlton, M.; Lee, W. H.; Wu, Q.; Li, H.; Zhu, Y.; Wu, Y.; Piner, R.; Ruoff, R. S. *ACS Nano* **2011**, *5*, 7656−7661.
(17) Zhou, X.; Yin, Y.-X.; Cao, A.-M.; Wan, L.-J.; Guo, Y.-G. *ACS Appl. Mater. Interfaces* **2012**, *4*, 2824−2828.
(18) Stankovich, S.; Dikin, D. A.; Dommett, G. H. B.; Kohlhaas, K. M.; Zimney, E. J.; Stach, E. A.; Piner, R. D.; Nguyen, S. B. T.; Ruoff, R. S. *Nature* **2006**, *442*, 282−286.
(19) Ding, F.; Ji, H.; Chen, Y.; Herklotz, A.; Dörr, K.; Mei, Y.; Rastelli, A.; Schmidt, O. G. *Nano Lett.* **2010**, *10*, 3453−3458.
(20) Zhang, K.; Han, P.; Gu, L.; Zhang, L.; Liu, Z.; Kong, Q.; Zhang, C.; Dong, S.; Zhang, Z.; Yao, J.; Xu, H.; Cui, G.; Chen, L. *ACS Appl. Mater. Interfaces* **2012**, *4*, 658−664.
(21) Yu, Y.; Gu, L.; Zhu, C.; van Aken, P. A.; Maier, J. *J. Am. Chem. Soc.* **2009**, *131*, 15984−15985.
(22) Venkateswara Rao, C.; Leela Mohana Reddy, A.; Ishikawa, Y.; Ajayan, P. M. *ACS Appl. Mater. Interfaces* **2011**, *3*, 2966−2972.
(23) Zhang, L. S.; Jiang, L. Y.; Yan, H. J.; Wang, W. D.; Wang, W.; Song, W. G.; Guo, Y. G.; Wan, L. J. *J. Mater. Chem.* **2010**, *20*, 5462−5467.
(24) Wang, B.; Wu, X.-L.; Shu, C.-Y.; Guo, Y.-G.; Wang, C.-R. *J. Mater. Chem.* **2010**, *20*, 10661−10664.
(25) Yang, S.; Cui, G.; Pang, S.; Cao, Q.; Kolb, U.; Feng, X.; Maier, J.; Müllen, K. *ChemSusChem* **2010**, *3*, 236−239.

(26) Wang, H.; Cui, L. F.; Yang, Y.; Sanchez Casalongue, H.; Robinson, J. T.; Liang, Y.; Cui, Y.; Dai, H. *J. Am. Chem. Soc.* **2010**, *132*, 13978−13980.
(27) Johnson, C. S.; Li, N.; Lefief, C.; Vaughey, J. T.; Thackeray, M. M. *Chem. Mater.* **2008**, *20*, 6095−6106.
(28) Park, K.; Song, C.; Stephan, A.; Jeong, S.; Nahm, K.; Oh, S.; Kim, Y. *J. Mater. Sci.* **2006**, *41*, 7628−7635.
(29) Jiang, K.-C.; Xin, S.; Lee, J.-S.; Kim, J.; Xiao, X.-L.; Guo, Y.-G. *Phys. Chem. Chem. Phys.* **2012**, *14*, 2934−2939.
(30) Liu, J.; Reeja-Jayan, B.; Manthiram, A. *J. Phys. Chem. C* **2010**, *114*, 9528−9533.